Hindawi
Advances in Materials Science and Engineering
Volume 2022, Article ID 6608596, 12 pages
https://doi.org/10.1155/2022/6608596

Research Article

An Investigation on Effects by Adding Cerium and Lithium on Mechanical and Metallurgical Properties of AZ91D + XCe + XLi Cast Mg Alloy

R. Krishnan[1], **S. Manivannan**[2], **A. Daniel Das**[3], **C. Ramesh Kannan**[4] and **Bashyam Sasikumar**[5]

[1]*Research Scholar,Department of Mechanical Engineering, Karpagam Academy of Higher Education, Coimbatore, Tamilnadu, India*
[2]*Centre for Material Science, Karpagam Academy of Higher Education, Coimbatore, Tamilnadu, India*
[3]*Department of Mechanical Engineering, Karpagam Academy of Higher Education, Coimbatore, Tamilnadu, India*
[4]*Department of Mechanical Engineering, Dr. Navalar Nedunchezhiyan College of Engineering, Tholudur, Tamilnadu, India*
[5]*Faculty of Mechanical Engineering, Arba Minch University, Arba Minch, Ethiopia*

Correspondence should be addressed to S. Manivannan; manivannan.s@kahedu.edu.in and Bashyam Sasikumar; bashyam.sasikumar@amu.edu.et

Received 18 February 2022; Revised 14 March 2022; Accepted 18 March 2022; Published 30 March 2022

Academic Editor: Samson Jerold Samuel Chelladurai

In this research work, the analysis of mechanical and metallurgical properties of AZ91D + XCe + XLi cast magnesium (Mg) alloys in adding cerium (Ce) and lithium (Li), where *X* can be varied. The destructive tests viz. mechanical test, tensile strength test, and microhardness test are used to investigate mechanical properties of AZ91D alloy in adding various weight percentages viz. 0.5, 1, 2, of Ce and Li. This result of this present investigation reveals that there will be refinement of grain size on AZ91D alloy in adding Ce and Li. The formation of second phase Al2Ce that has superior melting point, changes the distribution of the phase Mg17Al12 from a continuous network morphological transition to a tiny and dispersive distribution along the grain boundary. Furthermore, adding Li to the AZ91D magnesium alloy lowers the corrosion current density in a 3.5 percent NaCl solution, improving the alloy's corrosion resistance. The results show that the AZ91D magnesium alloy, which contains 0.5 percent Ce + 1.0wt.%, outperforms other magnesium alloys.

1. Introduction

By analysing the mechanical properties of Magnesium Alloys, the behaviour of the material has excellent dimensional stability, excellent and machinability. It can be used in electronic industries since the Mg Alloy has excellent strength to the weight ratio, high conductivity in thermal applications. The same alloy has been suggested to manufacturing Automotive and Aerospace components because Mg alloy is a low density material [1]. Nowadays, Magnesium alloys have been used in manufacturing automobile components viz. Engine Blocks, Gearbox Cases, Cylinder head covers etc., where the composite material Mg-Al is used to fabricate crankcases. In addition to that, Magnesium alloys are excellent in corrosion and wear resistance. Magnesium Alloys encounter tremendous studies with surface modification procedures which includes ionization, anodizing, laser melting, plasma electrolysis, oxidation & laser cladded coatings etc. [2]. The approaches are successful in increasing Mg alloy surface characteristics, but enhancing Mg alloy bulk properties is just as vital, if not more significant [3]. If the corrosion and wear resistance of these materials cannot be enhanced, failure of components made of them will surely increase once the surface coating is destroyed. Alloying, heat treatment, and the deformation process are all popular procedures for improving Mg alloy properties, with alloying being the most fundamental process [4]. Where, Mg alloys with rare Earth elements

including Y, La, Ce, Nd, and Gd have been proven to have improved mechanical properties and corrosion resistance.

2. Experimental Methods

The material employed in this study is a commercial AZ91D Mg alloy with a Mg-9Al-1Zn composition. The chemical composition of the magnesium alloys along with Yttrium addition is shown in Table 1. The first step of the experiment is casting of AZ91D alloy which is the base material and the addition of Li and Ce to it in the varying %ages like 0.5, 1, 2.0 wt.%. Casting of these alloys is done in Magnesium stir casting furnace [5]. Metals that have been carefully weighed at 400°C, the crucible is filled with Magnesium Cerium master alloy and Al [6]. A gas mixture of 99% Ar and 1% SF6 is introduced into the crucible at a rate of 0.25 m^3/hr at 650°C, and the temperature is maintained at 700°C (Mg–Al Melts). At this point, Li is added, inoculants are introduced after 5 minutes (1 minute is allowed to ensure inoculants melt), and the stirrer assembly is plunged into the melt [7]. The stirring is done with the predefined parameters and the molten metal is poured into the die. After the completion of the castings the alloys has been cut into different dimensions based on the specifications specified in different experiments conducted according to ASTM Standards [8]. To perform optical microscopy, the cut specimens were cold mounted, polished, and etched for 5–10 seconds. Optical microscopy was used to examine the microstructures of the specimens [9]. Microhardness test of the specimens has been conducted using microhardness tester. The test has been performed to identify the Density of the alloys as per ASTM D792 standards. To evaluate the influence of refining on phase size, a Scanning Electron Microscopy (SEM) paired with an Energy Dispersive Spectrometer was used to examine both refined and unrefined alloys (EDX) [10]. X-Ray Diffraction of the specimens is also completed to analyze the different phases present and also to find new phases that are formed due to addition of Yttrium in various composition [11]. To find the better corrosion resistance of the alloy corrosion tests like potentio dynamic polarization test and immersion tests has been conducted. Table 1 shows the chemical composition of magnesium alloys used in the research work.

3. Results and Discussion

3.1. Effects of Cerium and Lithium on AZ91D Mg Alloy. The microstructural studies were carried out by polishing the samples to mirror surface finish using emery papers and disc polishing machines and then etched properly by using oxalic acid solution for 10–15 seconds. The optical microscope was used to find the microstructure [12].

3.2. Microstructure of As-Cast AZ91D. Figure 1 depicts the AZ91D alloy's as-cast microstructure taken using Leica DM500. According to microstructure studies, the (Mg17Al12)-phase is the second phase in the AZ91D alloy. Mg17Al12 represents the network structure. Because it has a larger corrosion potential than the surrounding bulk material, the phase promotes the corrosion of magnesium (Mg) alloy as a cathode [13]. The Mg-Al phase diagram predicts the interaction of two phases at 9% Al: A Mg-rich phase and a phase that contains the intermetallic complex Mg17Al12. At roughly 620°C, the phase begins to solidify as the alloy cools from its liquid form. At around 540°C, solidification is complete, and the material is totally in the phase at this temperature. The phase begins to precipitate at 300°C, and the mass fraction of this secondary phase continues to expand as the material cools [14]. The phase makes up roughly 7.5% of the substance at temperatures below 100°C.

3.3. Microstructure of AZ91D + X%Ce + X%Li. A rare Earth element cerium (Ce) refines AZ91D significantly. Li and Ce are frequently concentrated near the solid-liquid boundary during the solidification process, which can greatly stifle phase expansion. Also, a black dot like phase dispersed in grains can be observed, which can be proved to be Al_2Ce compound by XRD Analysis [15]. It can be seen from Figure 2, thus by adding Li and Ce α-Mg dendrites and $Mg_{17}Al_{12}$ has been refined and the finest refinement is obtained in 0.5 wt.% of Li added alloy. Microstructure refinement is generally thought to be highly beneficial in improving the mechanical characteristics of magnesium alloys [16].

3.4. SEM and EDX Analysis. Figure 3 shows the results of SEM analysis of the AZ91D alloy taken in JSM-7900F. The EDX patterns of -phase are shown in the diagrams below. The highlighted white phase is largely formed of Mg, Al, Zn, Ce, and Li, showing a composition change from the usual Al-Mg phase, according to EDS patterns. The phase undergoes some compositional modifications in addition to microstructure refinement. These exceptional adjustments could have a good influence on the mechanical characteristics and corrosion resistance of the Ce and Li modified AZ91D magnesium alloy, but additional study is needed, which will be done using XRD Analysis [17]. The SEM and EDX investigation of the AZ91D + 1.0wt% Ce + 1.0wt% Li alloy are shown in Figure 4. Figure 4 shows the results of the SEM and EDX study of the AZ91D + 1.0wt% Ce + 1.0wt% Li alloy. With the addition of Ce, the microstructure of the AZ91D magnesium alloy is greatly refined, as seen in Figure 4. Furthermore, the Al4Ce phase appears at the grain boundary, and the composition of the typical Al-Mg phase changes dramatically [18].

3.5. X-Ray Diffraction. Figure 5 shows the XRD analysis of AZ91D + 0.5wt.% Ce + 0.5wt.% Li, AZ91D + 1.0wt.% Ce + 1.0wt.% Li and AZ91D + 2.0wt.% Ce + 2.0wt.% Li alloys taken in X'Pert3 MRD and the graph is plotted using pcpdfwin. XRD analysis confirmed the presence of new phases in the alloys [19]. XRD identified only α-Mg, β-$Mg_{17}Al_{12}$ in AZ91D and found additional phase containing Li in the remaining alloys. Total four phases were found α, β, Mg–Al intermetallic and Al_4Ce. In AZ91D alloy

Table 1: Chemical composition of magnesium alloys used in this work.

Experimental alloys	Al (%)	Mn (%)	Zn (%)	Si (%)	Ce (%)	Li (%)	Fe (%)	Mg (%)
AZ91D	8.8	0.02	0.4	0.1	-	-	0.005	Balance
AZ91D + 0.5 Ce + 0.5Li	8.73	0.15	0.33	0.07	0.45	0.43	0.005	Balance
AZ91D + 1.0 Ce + 1.0Li	8.85	0.08	0.52	0.15	0.91	0.852	0.04	Balance
AZ91D + 2.0 Ce + 2.0Li	8.63	0.10	0.80	0.18	1.812	1.83	0.004	Balance

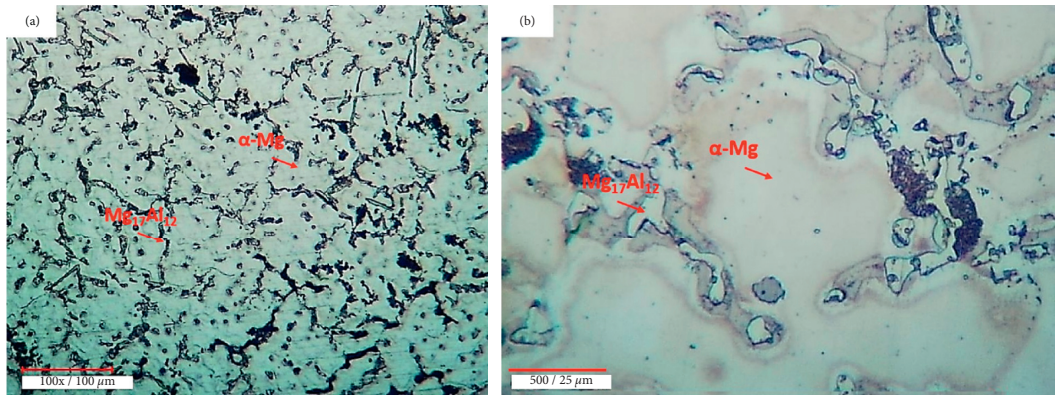

Figure 1: Microstructure of AZ91D: (a) lower magnification (100 μm); (b) higher magnification (25 μm).

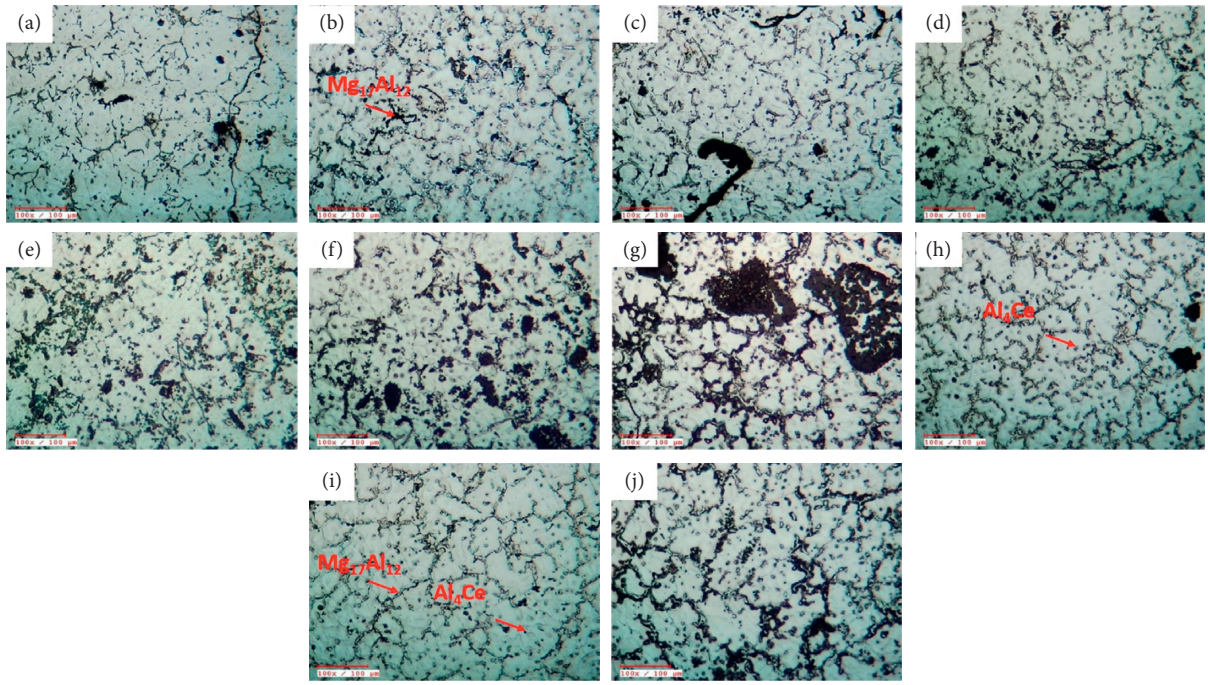

Figure 2: Microstructure of AZ91D + Xwt.%Ce + Xwt.%Li.

only 3 phases were found and the Li containing phase is absent. In 0.5 wt.% of Li and Ce alloy due to little amount of lithium addition only small peaks of Li can be found [20]. In 2.0 wt.% of Li and Ce due to significant amount of lithium addition many numbers of peaks can be found.

3.6. Tensile Test. Sub-size samples were prepared in accordance with ASTM E8 standard shown in Figure 6. Tensometer testing equipment has been used for testing the alloys like AZ91D + xLi + xCe. Figure 7 shows the graphical representation of Tensile test results [21]. The results found that the yield strength of the alloys has been increased by alloying with cerium. Addition of lithium increases yield due to the formation of solid where $X = 0.5$, 1.0 and 2.0. The highest tensile strength has been found in alloy of 0.5 wt.% Li and 2.0 wt.% of Ce alloy due to its precipitation of hard phase of Al_4Ce. But in alloy of 1.0 wt.% Li and 1.0wt.% of Ce alloy show the better results in yield strength, UTS and % of Elongation value due to its uniform distribution of rare

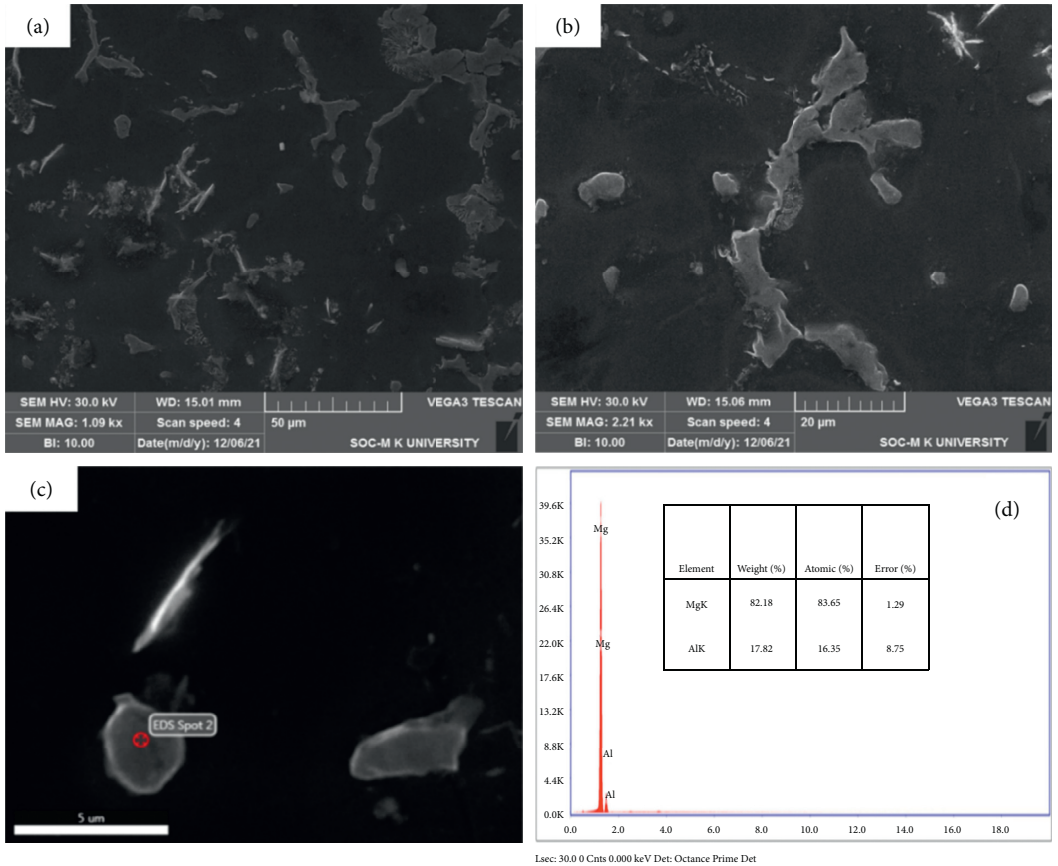

Figure 3: SEM and EDX Analysis of AZ91D alloy.

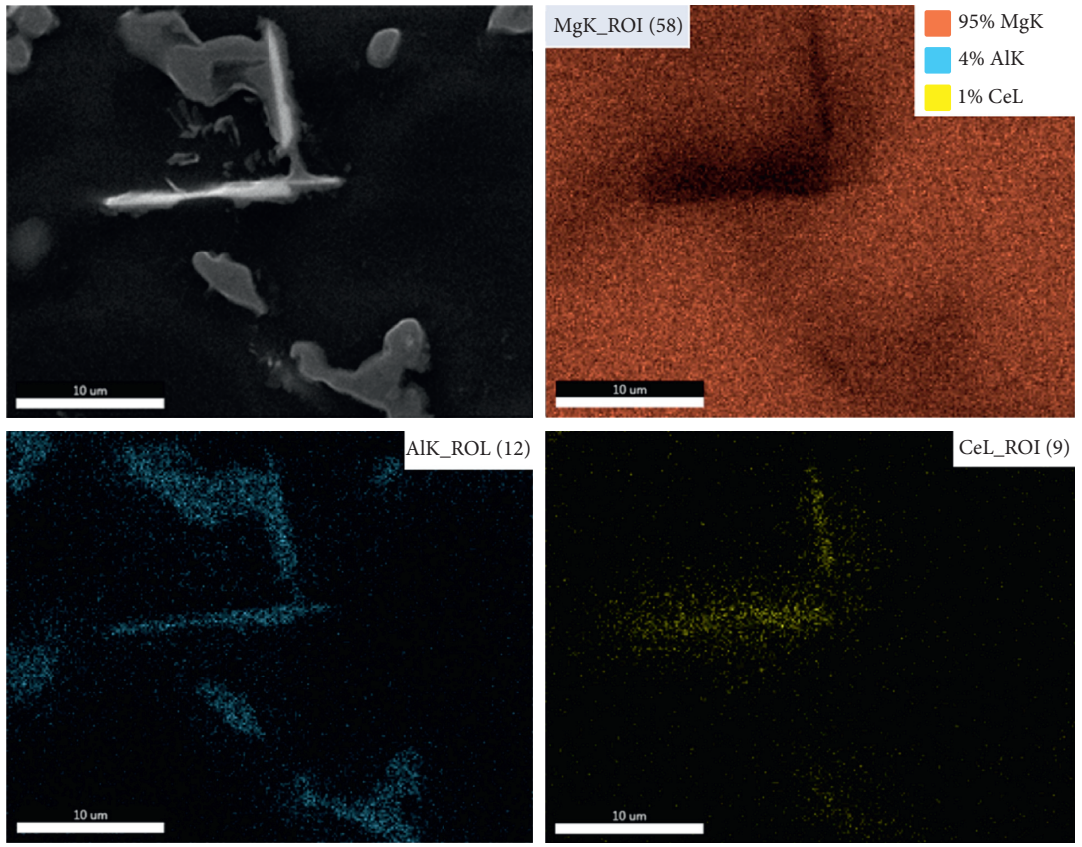

Figure 4: SEM and EDX analysis of AZ91D + 1.0wt.% Ce + 1.0wt.% Li.

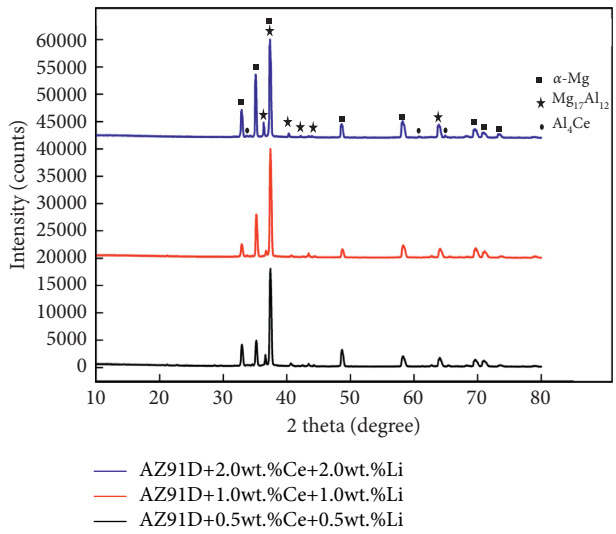

Figure 5: XRD Analysis of AZ91D + X wt.% Ce + X wt.% Li.

Figure 6: Tensile test sample.

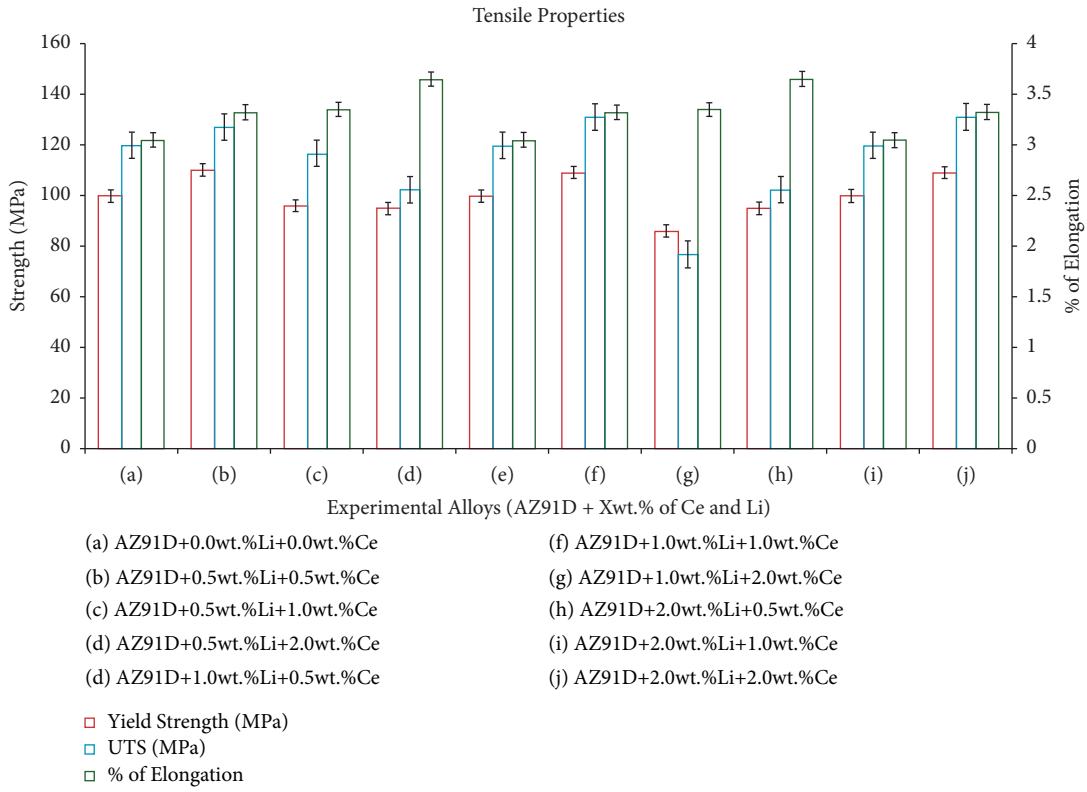

Figure 7: Graphical Histogram of Tensile test results.

Earth combination of phases along the α-Mg grain boundary which is confirmed in SEM analysis [22]. Figure 8 shows the fractography Analysis of AZ91D + 1.0wt.% C e +1.0wt.% Li confirms the dimples and hard A_4Ce phase. In further addition α-Mg grain refined in alloy g, also the formation β ($Mg_{17}Al_{12}$)-phase and Al4Ce phase precipitated become

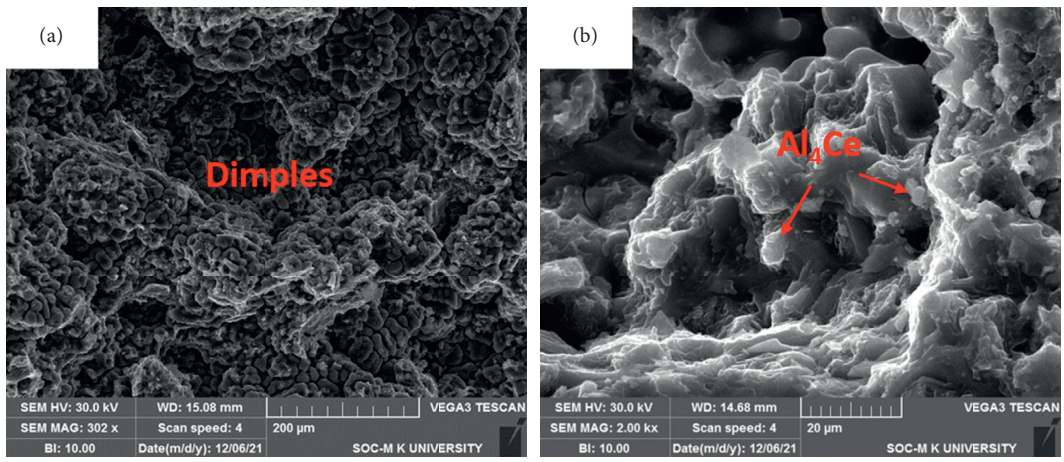

Figure 8: Fractography analysis of AZ91D + 1.0wt.% Ce + 1.0wt.% Li.

coarsen. So, from tensile results it is found that the alloys of g, h, and i decreases in yield strength and UTS.

3.7. Microhardness Test. Microhardness testing equipment is used for testing of the alloys AZ91D + xLi + xCe. Microhardness results are shown in Figure 9. The results found that the hardness of the alloys has been increased by alloying with Yttrium. Addition of Yttrium increases hardness due to the formation of solid where $X = 0.5$, 1.0 and 2.0. The solution strengthening phase Al_4Ce, phase is harder compared to α-Mg and β ($Mg_{17}Al_{12}$)-phase. With increase in Ce content more than 0.5 wt.% Al_2Ce formation decreases compared to β ($Mg_{17}Al_{12}$)-phase. So, from hardness test it is found that among all the alloys AZ91D + 0.5wt.% Ce is found to be with highest hardness [23].

3.8. Corrosion Immersion Test. To remove corrosion products from the coupons' surface, the submerged specimens were cleaned with inhibited acid (15 percent HCl) according to ASTM G1 (Standard Practice for Preparing, Cleaning, and Evaluating Corrosion Test Specimens). After that, the vouchers were cleaned under running water. After that, the coupons were dried in a 70°C oven for 15 minutes. They were dried, refrigerated in a desiccator, and weighed using a Mettle Toledo weighing scale (New Classic ML 204, Switzerland) to a consistent weight [24]. The discrepancy between the starting weight and the weight of the retrieved coupons before cleaning indicated that metal loss occurred during the course of the exposure. The ASTM G14 standard uses an immersion test to determine the corrosion rate of samples using the weight loss approach. The corrosion rate values for the prepared samples are shown in Table 2.

The corrosion rate was computed based on the assumption of homogenous corrosion throughout the coupons' whole surface. The weight loss was used to compute the corrosion rate in millimetres per year using the formula indicated in equation (1).

$$\text{corrosion rate} = \frac{(\text{WL} * K)}{(D * A * t)}, \tag{1}$$

where WL: weight loss in gm, K: constant, D: density in g/cm^3, A: area in mm, t: time of exposure in hrs.

When the density of the alloys comprising 0.5wt. % Li + Ce, 1.0wt. % Li + Ce, and 2.0wt. % Li + Ce was compared to that of the basic AZ91D alloy, it was discovered that the density of the alloys containing 0.5wt. % Li + Ce, 1.0wt. % Li + Ce, and 2.0wt. % Li + Ce was lower. The corrosion rates and density test results are shown in Table 3. Table 2 shows the variance in corrosion rate of alloys with varying amounts of rare Earth cerium [25]. The corrosion rate of the alloys containing 0.5wt% Li + Ce, 1.0wt% Li + Ce, and 2.0wt% Li + Ce is significantly lower than that of AZ91D. This shows that rare Earth cerium can greatly improve the AZ91D alloy's corrosion resistance. This substantial increase might be due to the appearance of new Ce-containing phases, Al4Ce, on grain borders as well as in the grain interior. These new phases may increase the stability of the layer generated on the phase's surface, reducing corrosion attack. The corrosion rate increases somewhat as the quantity of rare Earth cerium in the alloy increases, and the addition of Li content beyond 1 wt. percent increases the corrosion rate, suggesting that too much rare Earth cerium may reduce the AZ91D alloy's corrosion resistance. Rare Earth cerium can increase the quantity of phase on grain boundaries and make them more continuous in magnesium alloys, as evidenced in microstructures, which could explain why rare Earth cerium can induce minimal corrosion on magnesium alloys [26].

4. Corrosion Investigation

4.1. Immersion Test. After immersion in 3.5% NaCl Solution, optical microscopy of 0.5wt. % Li + Ce, 1.0wt. % Li + Ce, and 2.0wt. % Li + Ce is shown in Figure 10.

The corrosion surfaces of AZ91D alloys showed two distinct characteristics: the runaway of the corrosion layer from the corrosion surface, as shown in 0.5wt% Li + Ce, and

(a) AZ91D+0.0wt.%Li+0.0wt.%Ce
(b) AZ91D+0.5wt.%Li+0.5wt.%Ce
(c) AZ91D+0.5wt.%Li+1.0wt.%Ce
(d) AZ91D+0.5wt.%Li+2.0wt.%Ce
(d) AZ91D+1.0wt.%Li+0.5wt.%Ce
(f) AZ91D+1.0wt.%Li+1.0wt.%Ce
(g) AZ91D+1.0wt.%Li+2.0wt.%Ce
(h) AZ91D+2.0wt.%Li+0.5wt.%Ce
(i) AZ91D+2.0wt.%Li+1.0wt.%Ce
(j) AZ91D+2.0wt.%Li+2.0wt.%Ce

Figure 9: Microhardness results.

Table 2: Corrosion Rates for different experimental alloys.

Experimental alloys	Weight loss (g)	Density (gm/cc)	K Factor	Area (cm^2)	*TOE (h)	Corrosion rate (mm/year)
AZ91D + 0 wt.%Li + 0wt.%Ce	0.201	1.777	8.76×10^4	7.8	72	17.64353635
AZ91D + 0.5wt.%Li + 0.5wt.%Ce	0.004	1.7664	8.76×10^4	5.7	72	0.48335664
AZ91D + 0.5wt.%Li + 1.0wt.%Ce	0.068	1.7762	8.76×10^4	6.3	72	7.393466463
AZ91D + 0.5wt.%Li + 2.0wt.%Ce	0.096	1.7764	8.76×10^4	3.66	72	17.96474235
AZ91D + 1.0wt.%Li + 0.5wt.%Ce	0.201	1.781	8.76×10^4	7.81	72	17.58137
AZ91D + 1.0wt.%Li + 1.0wt.%Ce	0.003	1.7824	8.76×10^4	5.17	72	0.396092982
AZ91D + 1.0wt.%Li + 2.0wt.%Ce	0.011	1.7832	8.76×10^4	6.13	72	1.224344867
AZ91D + 2.0wt.%Li + 0.5wt.%Ce	0.016	1.7864	8.76×10^4	3.62	72	3.010262107
AZ91D + 2.0wt.%Li + 1.0wt.%Ce	0.02	1.787	8.76×10^4	6.31	72	2.157981383
AZ91D + 2.0wt.%Li + 2.0wt.%Ce	0.024	1.7884	8.76×10^4	3.56	72	4.586360541

*TOE: time of exposure.

Table 3: Potentio dynamic polarization results.

Specimen	E_{corr}	I_{corr}
AZ91D + 0wt.%Ce and Li	−253.66	2.623×10^{-2}
AZ91D + 0.5 wt.%Ce and Li	−241.42	1.366×10^{-5}
AZ91D + 1.0 wt.%Ce and Li	−344.68	1.272×10^{-4}
AZ91D + 2.0 wt.%Ce and Li	−291.14	4.038×10^{-3}

severe pitting corrosion. The corrosion rate of alloys with 0.5wt% Li + Ce and 1.0wt% Li + Ce is in the middle. When lithium was added, pitting corrosion was avoided, demonstrating that it slows down the rate of corrosion [27].

4.2. Potentio Dynamic Polarization Test. The applied potential is raised over time in Potentio dynamic studies, and the current is continually measured. The current density is compared to the potential density. The corrosion current (I_{corr}) was calculated using the Tafel extrapolation method from the polarization curve. Figure 11 shows the polarization curves of AZ91D and cerium and lithium added alloys. The addition of Li to the AZ91D alloy progressively moves the corrosion potential towards a more positive state, lowering the corrosion rates estimated from corrosion current densities. The preceding findings are pretty consistent with the results of the Immersion testing.

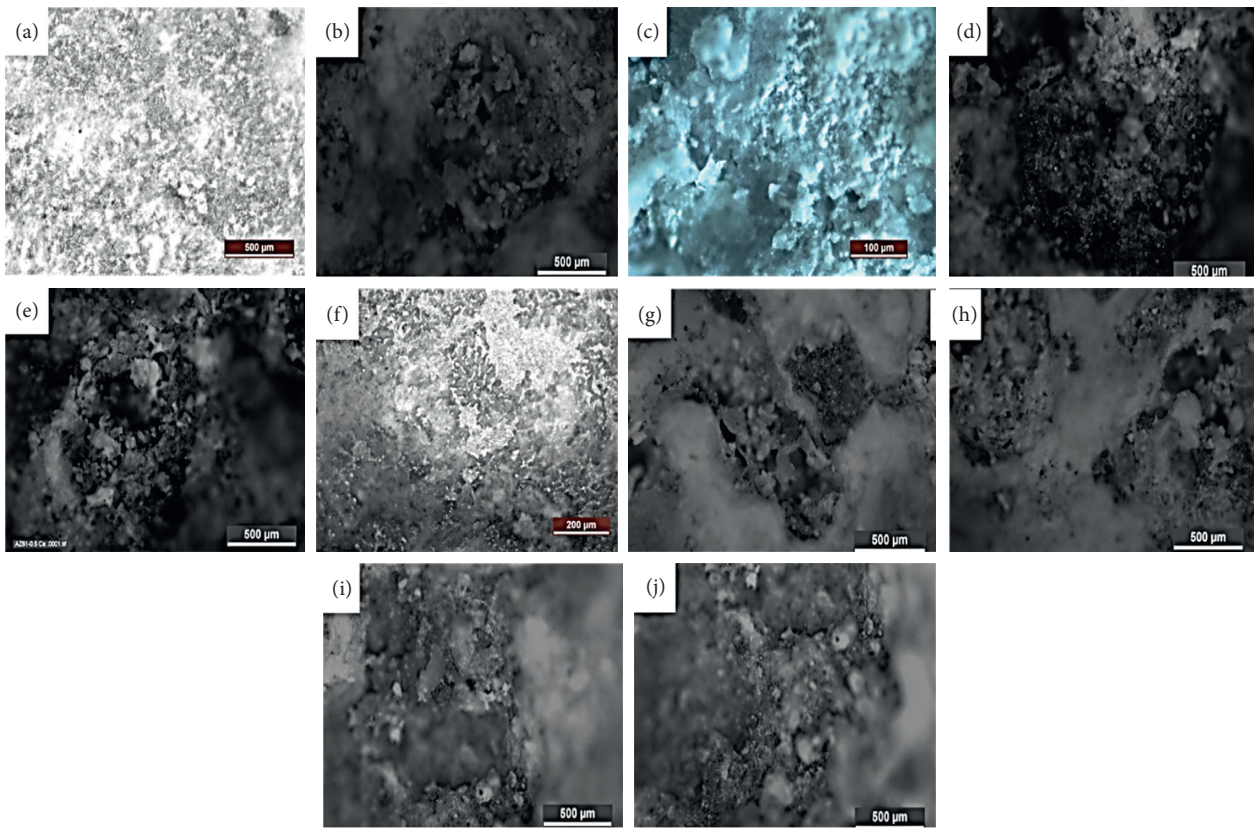

Figure 10: Microstructures after immersion test in 3.4 wt.% NaCl solution.

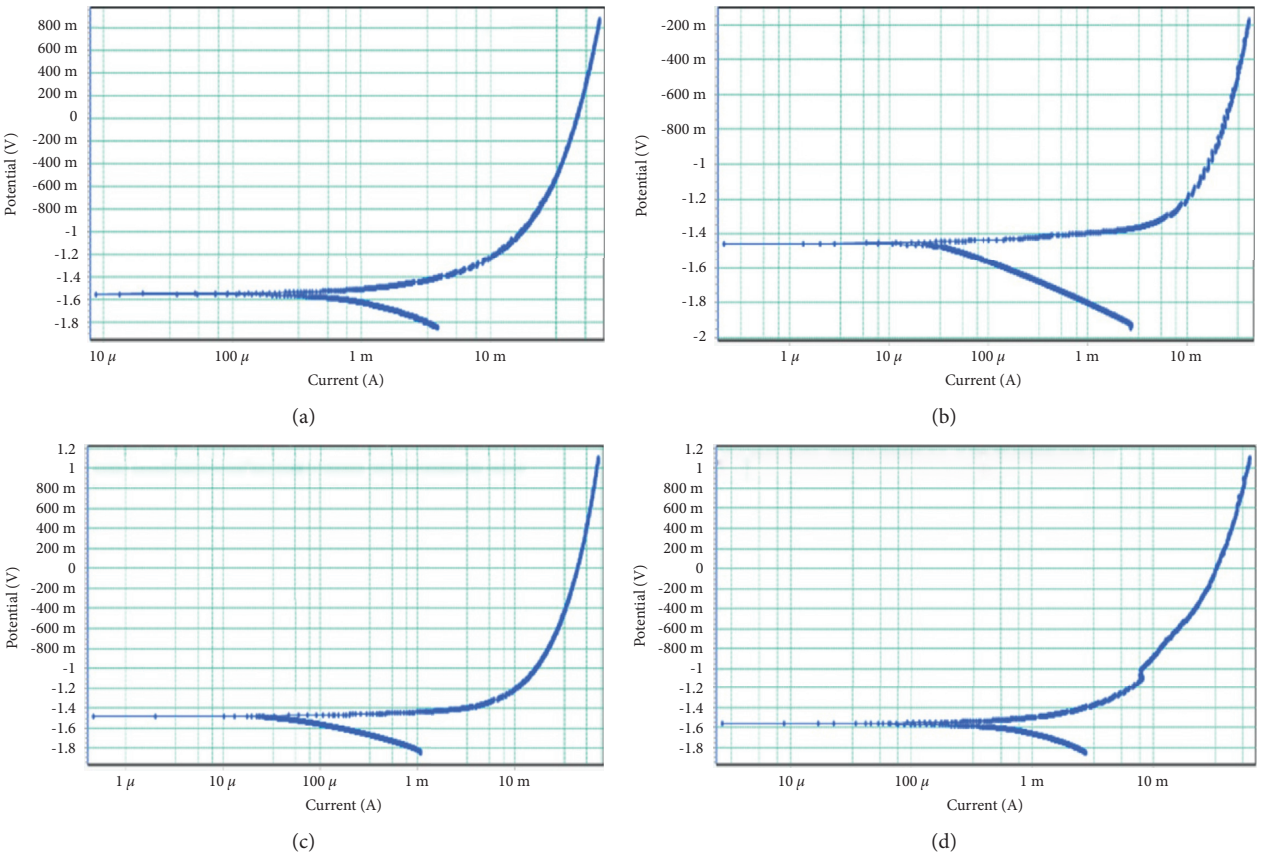

Figure 11: Potentio dynamic polarization results samples. (a) AZ91D + 0.0wt.%Li + 0.0wt.%Ce (b) AZ91D + 0.5wt.%Li + 0.5wt.%Ce (c) AZ91D + 1.0wt.%Li + 1.0wt.%Ce (d) AZ91D + 2.0wt.%Li + 2.0wt.%Ce.

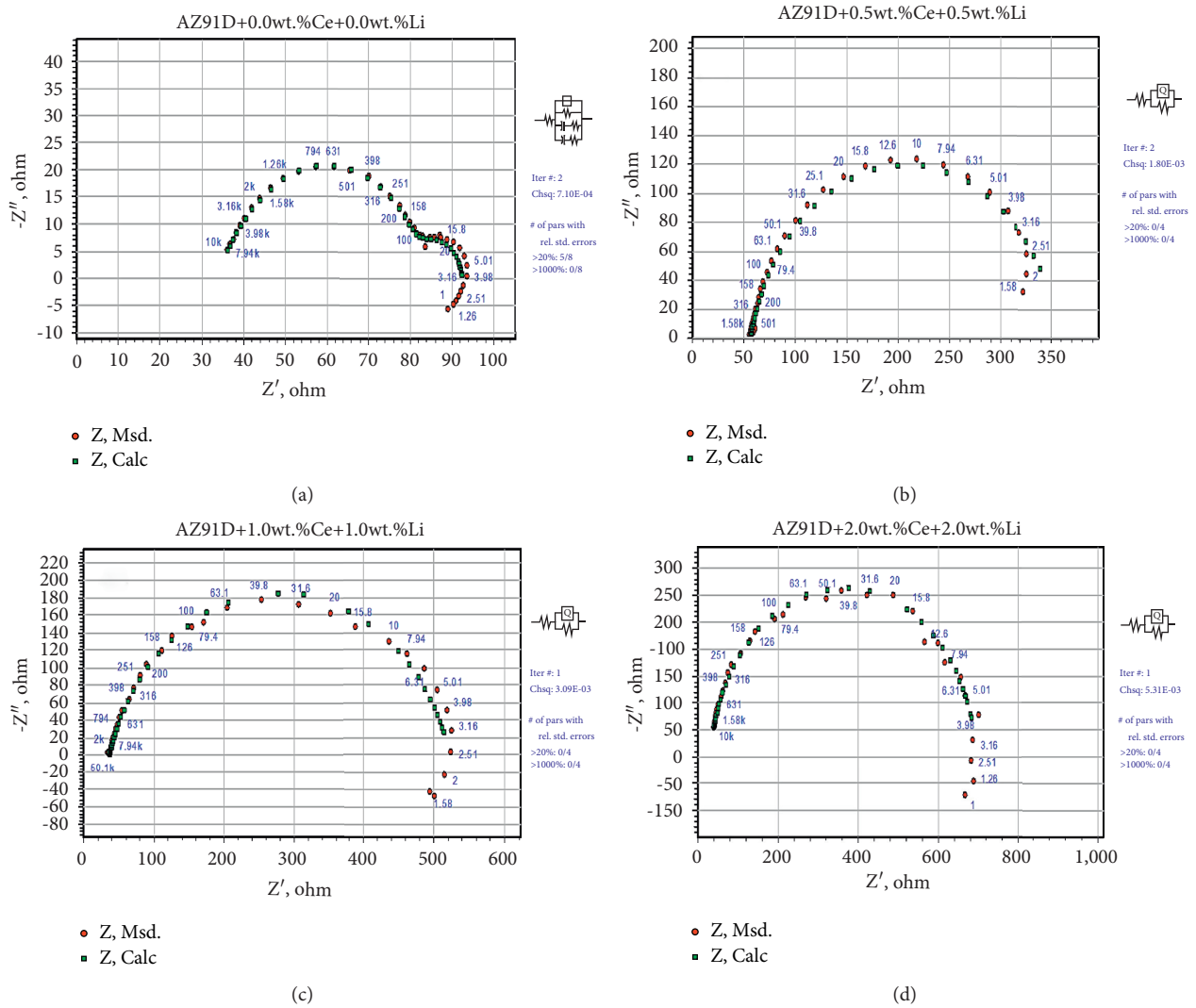

FIGURE 12: Nyquist plots and Bode impedance plots of as-cast and Ce and Li added AZ91D measured in a 3.5 wt% NaCl solution at their open-circuit potentials.

Table 3 shows the E_{corr} and Icorr values that were obtained.

As Icorr value is least for AZ91D + 0.5wt.% of Li + Ce, it is said to have high corrosion resistance followed by 0.5wt.% of Li + Ce, 1.0wt.% of Li + Ce and 2.0wt.% of Li + Ce. This shows that of all the alloy AZ91D is having lowest corrosion resistance.

4.3. Electrochemical Impedance Spectroscopy (EIS). The corrosion kinematics of as-cast AZ91D and various addition levels of lithium plus cerium AZ91D Mg alloy were originally investigated using EIS in a 3.5 wt percent NaCl solution. After immersing the specimen in 3.5 wt. percent NaCl solution for 15–17 mins, the electrochemical impedance spectroscopy test commenced. Figure 12 depicts the electrochemical impedance spectra of the as-cast AZ91D, cerium, and lithium added specimens in Nyquist plots. Capacitive loops are present in the as-cast state, however just one capacitive loop is present in the as-cast AZ91D specimen. The charge transfer resistance (*Rt*) of an electrode is connected to potential-dependent electrochemical processes at the solution-electrode interface, which is represented by the diameter of the first capacitive loop in the high frequency zone, during the test. The rate of electrode corrosion is lower when the distance or diameter is larger, and vice versa. The spectrum of the Ce + Li added specimen is about ten times that of the as-cast AZ91D specimen, demonstrating that molten salt treatment significantly enhances corrosion resistance. The EIS data was also used to generate Bode diagrams (Figure 13). The phase angle peak occurs at medium frequency for the various alloys, however the basic AZ91D alloy has not only a peak at the same frequency range, but also a "half" peak at high frequency [28]. It is plausible to assume that the double-peak pattern correlates to the two capacitive loops in Nyquist plots, implying that in the case of bare metal, there are at least two reactions. Electrical equivalent circuits (EEC) may be used to demonstrate the electrochemical mechanism and the

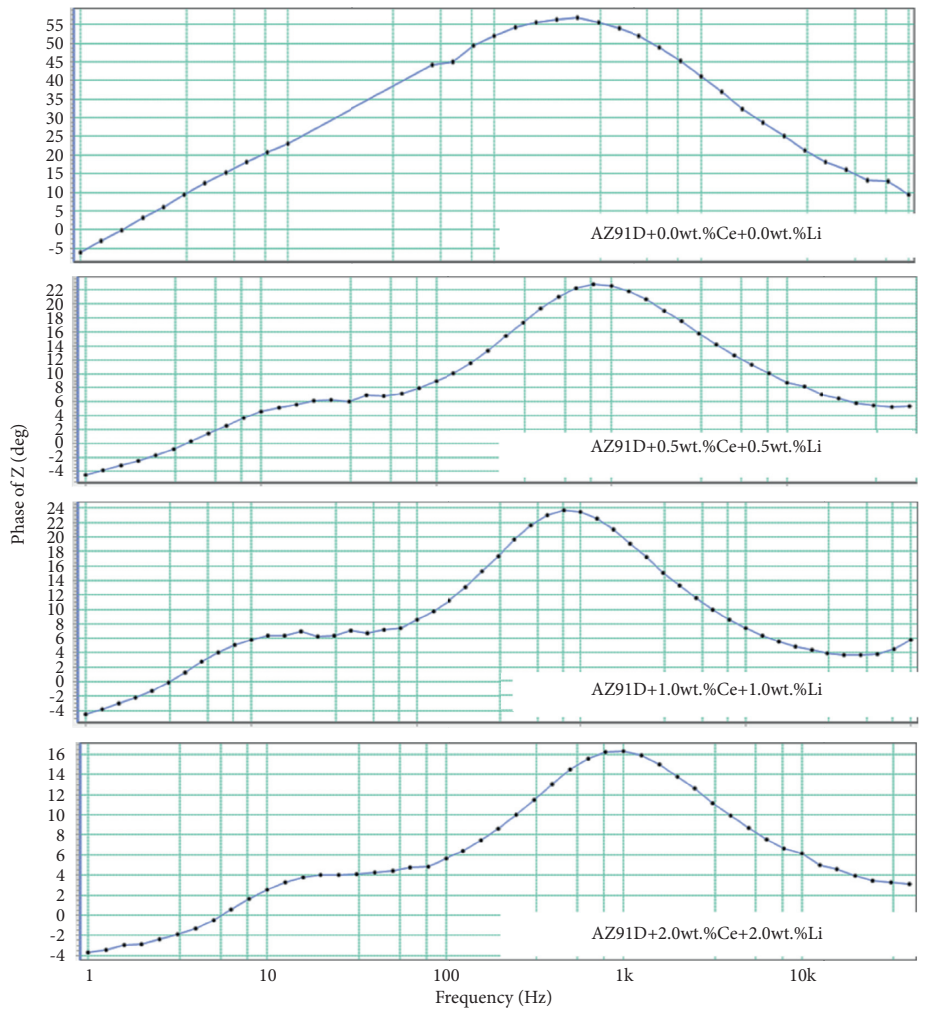

Figure 13: Bode plots for as-cast and Ce and Li added AZ91D measured in a 3.5 wt% NaCl solution at their open-circuit potentials.

formation of the Nyquist and Bode graphs [29]. The Faradaic process at low frequency involves both charge and mass transfer processes when the base AZ91D and cerium plus lithium added Mg alloy is submerged in the solution. The EEC depicted in Figure 12 can be used to describe the electrochemical system in this scenario. The phase angle and peak width of cerium plus lithium alloyed AZ91D Mg at medium frequency rose in lockstep with its EEC when compared to the Bode plots of AZ91D and cerium plus lithium added alloys. As a result, we can establish that the cerium plus lithium treated AZ91D Mg alloy shows a protective coating that is both stable and pleasing [30].

5. Conclusion

The conclusions on effects by adding cerium & lithium of AZ91D + XCe + XLi cast Mg alloy are as follows:

(i) Cerium and lithium additions to AZ91D magnesium alloy result in considerable microstructure refinement, including primary and eutectic phases.

(ii) The improved microstructure improves mechanical characteristics and corrosion resistance significantly.

(iii) The inclusion of cerium has boosted the hardness of the AZ91D alloy. This is because the Al4Ce hardening phase has formed.

(iv) The AZ91D alloys with 1.0wt.% of Li + Ce exhibiting good mechanical properties. The density of the cerium plus lithium added alloys has decreased significantly. [31].

(v) When compared to the base metal AZ91D, the corrosion resistance of Ce + Li alloys has improved. This has to do with the production of Al4Ce, the second rare Earth phase, which refines the phase from a continuous network shape to a small and dispersive dispersion along the grain boundary.

Data Availability

The data used to support the findings of this study are included within the article.

Conflicts of Interest

The authors declare that there are no conflicts of interest regarding the publication of this paper.

Acknowledgments

The publication of this research work is only for the academic purpose of Arba Minch University, Arba Minch, Ethiopia.

References

[1] Z. Wang, J. G. Wang, Z. Y. Chen et al., "Effect of Ce addition on modifying the microstructure and achieving a high elongation with a relatively high strength of as-extruded AZ80 magnesium alloy," *Materials*, vol. 12, no. 1, p. 76, 2019.

[2] A. K. Chaubey, S. Mohapatra, K. Jayasankar et al., "Effect of cerium addition on microstructure and mechanical properties of Al-Zn-Mg-Cu alloy," *Transactions of the Indian Institute of Metals*, vol. 62, no. 6, pp. 539–543, 2009.

[3] S. F. Liu, B. Li, X. H. Wang, W. Su, and H. Han, "Refinement effect of cerium, calcium and strontium in AZ91 magnesium alloy," *Journal of Materials Processing Technology*, vol. 209, no. 8, pp. 3999–4004, 2009.

[4] W. Yang, Z. Liu, and H. Huang, "Galvanic corrosion behavior between AZ91D magnesium alloy and copper in distilled water," *Corrosion Science*, vol. 188, Article ID 109562, 2021.

[5] F. Yan, B. Chen, J. Yao, D. Zhang, M. F. Yan, and Y. Zhang, "Characterization of microstructure and corrosion properties of AZ91D magnesium alloy surface-treated by coating-nitriding," *Journal of Materials Research and Technology*, vol. 14, pp. 1559–1568, 2021.

[6] H. Huang and W. Yang, "Corrosion behavior of AZ91D magnesium alloy in distilled water," *Arabian Journal of Chemistry*, vol. 13, no. 7, pp. 6044–6055, 2020.

[7] L.-J. Zhang, X.-B. Zhu, Z. Zhang, and J.-Q. Zhang, "Electrochemical noise characteristics in corrosion process of AZ91D magnesium alloy in neutral chloride solution," *Transactions of Nonferrous Metals Society of China*, vol. 19, no. 2, pp. 496–503, 2009.

[8] N. Rahulan, S. Gopalan, and S. Kumaran, "Effect of lithium on the mechanical behavior of magnesium," *Materials Today Proceedings*, vol. 18, pp. 2573–2580, 2019.

[9] M.-X. Zhang and P. M. Kelly, "Crystallography of Mg17Al12 precipitates in AZ91D alloy," *Scripta Materialia*, vol. 48, no. 5, pp. 647–652, 2003.

[10] G. Wang, D. Song, Y. Qiao et al., "Developing super-hydrophobic and corrosion-resistant coating on magnesium-lithium alloy via one-step hydrothermal processing," *Journal of Magnesium and Alloys*, 2021.

[11] R. V. Vignesh, R. Padmanaban, M. Govindaraju, and G. S. Priyadharshini, "Corrosion protection of magnesium alloys in simulated body fluids using nanophase Al2O3," in *Corrosion Protection at the Nanoscale Corrosion Protection at the Nanoscale*, pp. 21–45, Elsevier, Amsterdam, Netherlands, 2020.

[12] F. Witte, J. Fischer, J. Nellesen et al., "In vitro and in vivo corrosion measurements of magnesium alloys," *Biomaterials*, vol. 27, no. 7, pp. 1013–1018, 2006.

[13] P. Huang, J.-A. Latham, D. R. MacFarlane, P. C. Howlett, and M. Forsyth, "A review of ionic liquid surface film formation on Mg and its alloys for improved corrosion performance," *Electrochimica Acta*, vol. 110, pp. 501–510, 2013.

[14] R.-C. Zeng, X.-X. Sun, Y.-W. Song et al., "Influence of solution temperature on corrosion resistance of Zn-Ca phosphate conversion coating on biomedical Mg-Li-Ca alloys," *Transactions of Nonferrous Metals Society of China*, vol. 23, no. 11, pp. 3293–3299, 2013.

[15] S. Y. Jin, R. Z. Wu, J. X. Wang, G. X. Wang, K. Boris, and B. Sergey, "Corrosion behavior of Mg– Li alloys: a review," *Transactions of Nonferrous Metals Society of China*, vol. 31, no. 11, pp. 3228–3254, 2021.

[16] L. Guo, W. Wu, Y. Zhou, F. Zhang, R. Zeng, and J. Zeng, "Layered double hydroxide coatings on magnesium alloys: a review," *Journal of Materials Science & Technology*, vol. 34, no. 9, pp. 1455–1466, 2018.

[17] S. Chen, C. Yin, Yi Wang et al., "Developing polydopamine modified molybdenum disulfide/epoxy resin powder coatings with enhanced anticorrosion performance and wear resistance on magnesium lithium alloys," *Journal of Magnesium and Alloys*, 2021.

[18] H. Dong, S. Luo, W. Liu et al., "Size effect of the width of beta-Li phase on the ductility of magnesium-lithium dual-phase alloys," *Materials Science and Engineering A*, vol. 814, Article ID 141217, 2021.

[19] R. N. Abdullaev, R. A. Khairulin, Y. M. Kozlovskii, A. S. Agazhanov, and S. V. Stankus, "Density of magnesium and magnesium-lithium alloys in solid and liquid states," *Transactions of Nonferrous Metals Society of China*, vol. 29, no. 3, pp. 507–514, 2019.

[20] S.-Y. Jian and K.-L. Chang, "Effect of cerium ion on the microstructure and properties of permanganate conversion coating on LZ91 magnesium alloy," *Applied Surface Science*, vol. 509, Article ID 144767, 2020.

[21] V. Zahedi Asl, J. Zhao, M. J. Anjum, S. Wei, W. Wang, and Z. Zhao, "The effect of cerium cation on the microstructure and anti-corrosion performance of LDH conversion coatings on AZ31 magnesium alloy," *Journal of Alloys and Compounds*, vol. 821, Article ID 153248, 2020.

[22] S.-Y. Jian, Y.-C. Tzeng, M.-D. Ger et al., "The study of corrosion behavior of manganese-based conversion coating on LZ91 magnesium alloy: effect of addition of pyrophosphate and cerium," *Materials & Design*, vol. 192, Article ID 108707, 2020.

[23] C. Lin, C. Changguo, W. Ningning, W. Jimin, and D. Ling, "Study of cerium and lanthanum conversion coatings on AZ63 magnesium alloy surface," *Rare Metal Materials and Engineering*, vol. 44, no. 2, pp. 333–338, 2015.

[24] L. Chenghao, W. Shusen, H. Naibao, Z. Zhihong, Z. Shuchun, and R. Jing, "Effects of lanthanum and cerium mixed rare earth metal on abrasion and corrosion resistance of AM60 magnesium alloy," *Rare Metal Materials and Engineering*, vol. 44, no. 3, pp. 521–526, 2015.

[25] A. P. Loperena, I. L. Lehr, and S. B. Saidman, "Formation of a cerium conversion coating on magnesium alloy using ascorbic acid as additive. Characterisation and anticorrosive properties of the formed films," *Journal of Magnesium and Alloys*, vol. 4, no. 4, pp. 278–285, 2016.

[26] X. Wang, L. Zhu, X. He, and F. Sun, "Effect of cerium additive on aluminum-based chemical conversion coating on AZ91D magnesium alloy," *Applied Surface Science*, vol. 280, pp. 467–473, 2013.

[27] L. Li, J. Lei, S. Yu, Y. Tian, Q. Jiang, and F. Pan, "Formation and characterization of cerium conversion coatings on magnesium alloy," *Journal of Rare Earths*, vol. 26, no. 3, pp. 383–387, 2008.

[28] S. Tardif, R. Tremblay, and D. Dubé, "Influence of cerium on the microstructure and mechanical properties of ZA104 and ZA104+ 0.3 Ca magnesium alloys," *Materials Science and Engineering A*, vol. 527, pp. 29-30, 2010.

[29] X. Zhong, Q. Li, J. Hu, X. Yang, F. Luo, and Y. Dai, "Effect of cerium concentration on microstructure, morphology and

corrosion resistance of cerium-silica hybrid coatings on magnesium alloy AZ91D," *Progress in Organic Coatings*, vol. 69, no. 1, pp. 52–56, 2010.

[30] L.-L. Chang, J. Guo, and X.-J. Su, "Effect of Y on microstructure evolution and mechanical properties of Mg–4Li–3Al alloys," *Transactions of Nonferrous Metals Society of China*, vol. 31, no. 12, pp. 3691–3702, 2021.

[31] Y. Miao, C. Wang, M. Wang, H. Deng, P. Ma, and Z. Li, "Enhanced mechanical properties and isotropy of Mg-2Al-0.8Sn alloy through Ca addition," *Materials*, vol. 14, no. 24, p. 7557, 2021.